

Surface Modification of Iron for Corrosion Protection: Kinetics of Anodic Film Formation and Electroreduction

Željka Petrović¹, Mirjana Metikoš-Huković^{1,*}, Robert Peter², Mladen Petavić²

¹ Department of Electrochemistry, Faculty of Chemical Engineering and Technology, University of Zagreb, P.O. Box 177, 10000 Zagreb, Croatia

² Department of Physics and Center for Micro and Nano Science and Technologies, University of Rijeka, Omladinska 14, 51 000 Rijeka, Croatia

*E-mail: mmetik@fkit.hr

Received: 26 July 2012 / Accepted: 24 August 2012 / Published: 1 October 2012

The surface modification of Armco[®] iron for corrosion protection was performed by using the formation of the passive oxide film as well as the surface treatment by an ionic liquid. The band structure model was employed to explain the kinetics of oxide film growth and reduction in terms of point defects diffusivity. Low values of the diffusion coefficient and the concentration of anion vacancies as well as the high charge transfer resistance values point to high protecting properties of the passive oxide film in the wide potential range. Protection efficiency of the spontaneously formed oxide film at the open circuit potential (E_{OCP}) was markedly enhanced by adsorption of 1-butyl-3-methylimidazolium ($[C_4MIm]^+$) cations on a negatively charged iron surface. The nature and the chemical composition of the surface oxide film on iron in the dependence of the formation potential were studied by X-ray photoelectron spectroscopy (XPS). XPS results showed a clear lowering of the iron valence through the oxide film until metallic iron.

Keywords: iron, formation and reduction of oxide film, ionic liquids, EIS, XPS

1. INTRODUCTION

In a contact with humid air or near neutral and alkaline aqueous solutions the iron surface is covered by an oxide/hydroxide layer of a poor surface coverage, a low mechanical integrity, and a low corrosion resistance. Different types of corrosion protection have been used such as (i) inorganic conversion coatings (including oxide-, phosphate- and chromate-based coatings) and (ii) organic coatings produced by adsorption of organic molecules (corrosion inhibitors), by self-assembling of organic molecules, and coatings formed by adsorption of molecular ions (ionic liquids).

The majority of work in the first area is devoted to the study of oxide film formation/passivation and the characterization of the structural and electronic properties of the passive film, especially in near neutral borate buffer solutions [1-14]. There are several advantages of using this electrolyte solution: (a) the borate ions possess the adsorption affinity much smaller than other anions [14], (b) the oxide layer is chemically stable in a wide potential range [4], (c) the active to passive transition occurs with small current densities [2,3], and (d) the potential drop in the Helmholtz layer is constant and depends only on the pH, and any change of the electrode potential causes a change of the potential drop in the oxide [11].

During passivation, the ionic current is related to the number of defects in the oxide film, i.e., oxygen and cation vacancies, whose transport occurs under the influence of the electrostatic field. Macdonald's point defect model (PDM) uses the elementary vacancy generation and annihilation reactions at the metal|film and at the film|solution interfaces as the bases [15,16]. A key parameter in describing the transport properties of oxygen vacancies and cation vacancies, and hence the kinetics of film growth is the vacancy diffusivity (D_o), which appears in the Nernst-Planck equation for the flux and temporal dependence of the vacancy concentration. Furthermore, these defects in the passive film generate localized states, which can act as donors or acceptor levels. Such electronic levels in the band-gap can be assumed to have a decisive influence on the reactivity of passive interfaces. The Mott-Schottky (MS) analysis in conjunction with the PDM for passive films enables determination of the diffusion coefficient of oxygen vacancies in passive films [17]. The vacancy concentration can be as large as 10^{21} cm^{-3} , if assumed that the defects act as the dopants; oxygen vacancies and cation vacancies, indicating n-type and p-type conductivity, respectively [15-17].

The main goal of the corrosion studies is to understand the corrosion mechanism on materials investigated and to gain *know how* in their efficient corrosion protection. In this sense, the modification of an iron surface for corrosion protection using passive oxide films and the surface treatments by ionic liquids was studied. The semiconducting properties of the passive films were investigated in a borate buffer, pH 8.4, and correlated with their corrosion resistance.

2. EXPERIMENTAL PART

2.1. Materials and solutions

ARMCO[®] soft ingot iron, 99.8%, was obtained from Goodfellow, England. The 2 mm thick plate was cut into discs with the cross section area of 1 cm^2 that was used as a working electrode. Before each measurement the samples were successively ground with SiC paper (#600 to #1000 grit), ultrasonically cleaned in redistilled water, and degreased in acetone. A borate buffer solution, pH 8.4, was used as an electrolyte. The chemical composition of a borate buffer solution, which was prepared with redistilled water, was $0.3 \text{ mol dm}^{-3} \text{ H}_3\text{BO}_3$ (Kemika, p.a.) + $0.075 \text{ mol dm}^{-3} \text{ Na}_2\text{B}_4\text{O}_7 \times 10\text{H}_2\text{O}$ (Kemika, p.a.). The ionic liquid used in study was 1-butyl-3-methylimidazolium bromide, Sigma-Aldrich, $\geq 98.5\%$).

2.2. Electrochemical and X-Ray photoelectron spectroscopy measurements

All electrochemical measurements were performed at $25 \pm 2^\circ \text{C}$ in a standard three electrode cell (PAR, Corrosion Cell System, Model K47). Graphite rods were used as the counter electrode and the reference electrode, to which all potentials in the paper are referred, was an Ag | AgCl, 3.0 mol dm^{-3} KCl ($E = 0.210 \text{ V}$ vs. SHE) [18]. Prior to all measurements, the surface oxide layer was removed by cathodic polarization at -1.2 V for 60s. A Solartron potentiostat/galvanostat 1287 with FRA 1260 was used in these measurements.

Cyclic voltammetry (CV) measurements were carried out at a scan rate of 1 mV s^{-1} in a potential range from -1.2 to 1.0 V . Electrochemical impedance spectroscopy (EIS) measurements were performed in the frequency range between 10^5 and $5 \times 10^{-3} \text{ Hz}$ with an *ac* voltage amplitude of $\pm 5 \text{ mV}$. Prior to each measurement the electrode was stabilized at a chosen potential for 24 h. Impedance data were fitted by a suitable electrical equivalent circuit (EEC) model, employing the complex non-linear least squares (CNLS) fit analysis offered by the Solartron ZView[®] software [19]. The fitting quality was evaluated by the chi-squared and relative error values, which were in the order of 10^{-3} - 10^{-4} and below 4 %, respectively, indicating that the agreement between the proposed EEC model and the experimental data was very good.

Due to a well known frequency dispersion on a solid electrode surface the interfacial capacitance in this work has been expressed in term of the constant phase element (CPE) [20]. Its impedance can be defined as $Z(\text{CPE}) = [Q(j\omega)^n]^{-1}$, where Q is the constant, ω is the angular frequency, and n is the CPE exponent. The interfacial capacitance (C_i) is calculated using the expression given by Brug et al. [21]:

$$Q_i = C_i^n (R_{el}^{-1} + R_i^{-1})^{1-n} \quad (1)$$

where R_{el} is the ohmic resistance and R_i is the charge transfer resistance (R_{ct}).

The capacitance values of the iron|solution interface, needed for a Mott-Schottky (MS) analysis, were determined from the imaginary part of impedance (Z_{imag}). After the electrode stabilization for 24 h at a film formation potential (E_f), the potential was swept from E_f to the negative direction at a sweep rate of 50 mV s^{-1} to avoid the electroreduction of the oxide layer and change in the film thickness during the measurements. In the MS experiments, the imaginary part of the impedance was recorded as a function of the potential at a frequency 10^3 Hz . Our previous investigation of iron passivity [22] showed that the MS plot obtained at 10^3 Hz correlated well with that obtained by using a procedure that eliminated the influence of frequency dispersion [22]. From the measured values of Z_{imag} and the previously determined CPE exponents n , it was possible to calculate the CPE parameter Q , and then the interfacial capacitance by using Eq.(1).

The X-ray photoelectron spectra (XPS) were recorded in a UHV chamber (typical pressure in the 10^{-7} - 10^{-6} Pa range) of a SPECS system with the Phoibos MCD 100 electron analyser and monochromatized Al K_λ x-rays of 1486.74 eV . For the pass energy of 10 eV used in the present study, the total energy resolution was around 0.8 eV . The photoemission spectra were simulated with several sets of mixed Gaussian-Lorentzian functions with Shirley background subtraction.

3. RESULTS AND DISCUSSION

3.1. Electrochemical behaviour of iron in a borate buffer solution

The cyclic polarization behaviour of iron in a borate buffer solution, pH 8.4, is presented in Fig. 1. The CV features are nearly identical to those reported in many of the earlier studies [1-6]. The oxidation reduction processes occurring inside the characteristic potential regions can be inferred from the equilibrium potentials [24] and the composition studies of passive films on iron in borate buffer solutions [3,7-9].

Inside the potential region of the anodic current peak A_I iron oxidation takes place and the main reaction is the formation of a monolayer of hydrous $\text{Fe}(\text{OH})_2$, which has been considered responsible for the prepassivation of iron in a borate buffer solution [4,5]. The mechanism of this process was discussed extensively in the literature [10]. The release of Fe^{2+} ions was detected at anodic potentials corresponding to the current peak A_I [3,4,6].

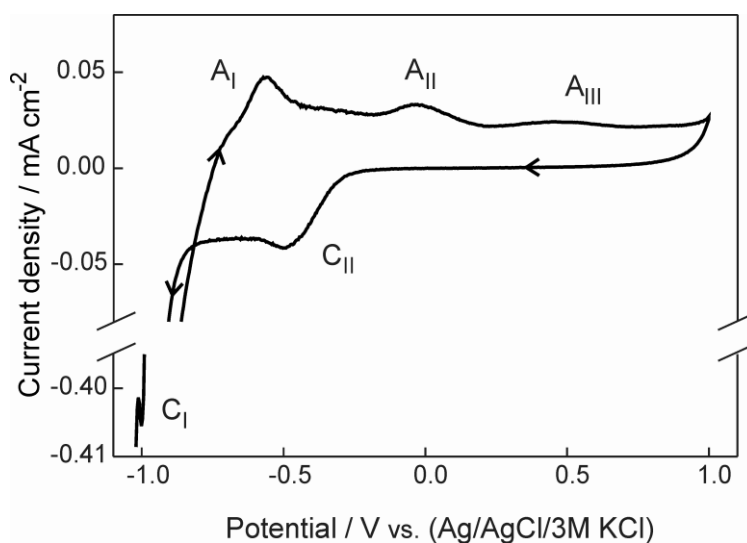


Figure 1. The cyclic voltammogram of the iron electrode in a borate buffer solution, pH 8.4, $\nu = 1 \text{ mVs}^{-1}$.

The broad current peak A_{II} can be considered as two overlapping current peaks [4]. At more negative potentials of A_{II} , the Fe^{2+} ions, generated during active-passive transition, can be oxidised to form a deposit of Fe(III) hydrated oxide, most frequently attributed to FeOOH [3,6,11]. By increasing anodic potential, i.e., at higher potentials of A_{II} , the solid state oxidation of Fe(II) oxide/hydroxides into Fe(III) oxide/hydroxide takes place. During this process, a small release of Fe^{3+} ions from the passive layer was registered [6]. XPS measurements performed on Fe in a borate buffer, pH 8.4, by Sieber et al. [9] have shown that oxygen inside the surface layer is present as O^{2-} and OH^- ions and the latter one, i.e, iron hydroxide is located in the outer part of the surface film, while iron oxide(s) in the inner layer. Therefore it has been widely accepted that the passive films formed at potentials of current peak A_{II} are of a bilayer structure consisting of an inner layer that is similar to Fe_3O_4 and/or $\gamma\text{-Fe}_2\text{O}_3$

and an outer layer of an as yet unknown Fe(III)-oxide/hydroxide (Raman peak at 560 cm^{-1}) [7]. By increasing anodic potential during a current plateau A_{III} , a thickness of the oxide layer increases [9] as well as the amount of Fe(III) species responsible for the Raman peak at 560 cm^{-1} .

The cathodic branch of the CV shows two current maxima; the first one (C_{II}) corresponds to the electroreduction of Fe(III) iron species, while the second one (C_{I}) results from the electroreduction of Fe(II) iron species, which proceeds together with the hydrogen evolution reaction [9,12]. The mechanisms of these processes are discussed in the section 3.4.

3.2. Semiconducting properties of the passive film on iron

First, we will present and discuss the electronic properties of the passive oxide film anodically formed on iron due to the following reasons: (i) a deep understanding of the electronic properties of the surface film is needed to predict long-term corrosion properties of iron and (ii) the band structure model was employed in this work to explain the oxide film growth and electroreduction (cathodic decomposition).

The MS analysis was applied to identify the electronic (semiconducting) properties of the passive films on iron in a borate buffer solution, pH 8.4 as a function of the formation potential across the entire passive range. MS experiments (capacitance measurements) were performed under conditions in which electronic conductivity of the passive film prevails and the space charge layer is formed creating a strong electric field at the solid|liquid interface, i.e. creating the barrier for the corrosion processes.

The value of the interfacial capacitance (C_{i}), obtained according to the procedure described in the Experimental part, consists of the space charge capacitance (C_{SC}) and the Helmholtz layer capacitance (C_{H}), and is equal to $(C_{\text{SC}}^{-1} + C_{\text{H}}^{-1})^{-1}$, under assumption that the contribution from the surface states can be neglected. Since the C_{i} values determined using Eq. (1) are much smaller than C_{H} for iron in a borate buffer solution, pH 8.4, ($C_{\text{H}} = 134\text{ }\mu\text{F cm}^{-2}$ [7]), the measured capacitance is approximately equal to C_{SC} . According to MS theory [25], the space charge capacitance of n- and p-type semiconductors is given by Eq. (2) and Eq. (3), respectively:

$$\frac{1}{C_{\text{SC}}^2} = \frac{2}{\varepsilon\varepsilon_0 e N_{\text{D}}} \left(E - E_{\text{fb}} - \frac{kT}{e} \right) \quad (2)$$

$$\frac{1}{C_{\text{SC}}^2} = \frac{-2}{\varepsilon\varepsilon_0 e N_{\text{A}}} \left(E - E_{\text{fb}} - \frac{kT}{e} \right) \quad (3)$$

where ε_0 is the vacuum permittivity ($8.85 \times 10^{-14}\text{ F cm}^{-1}$), ε is the dielectric constant of iron oxide ($\varepsilon = 30$ [26]), e is the electron charge ($1.602 \times 10^{-19}\text{ C}$), N_{D} and N_{A} are the donor and acceptor density in the passive film, respectively, E is the applied potential, E_{fb} is the flat band potential, k is the Boltzman constant ($1.38 \times 10^{-23}\text{ J K}^{-1}$), and T is the absolute temperature (298 K). For both n- and p-

type semiconductors, the C_{sc}^{-2} vs. E dependence should be linear with a slope that is inversely proportional to the donor/acceptor density.

As an example of MS analysis, Fig. 2 represents the C_{sc}^{-2} vs. E dependence measured on iron passivated at several potential values inside the current peak A_{III} for 24 h. The positive slope of the MS plots implies that passive films on iron formed at potentials inside the region A_{III} behave as an n-type semiconductor.

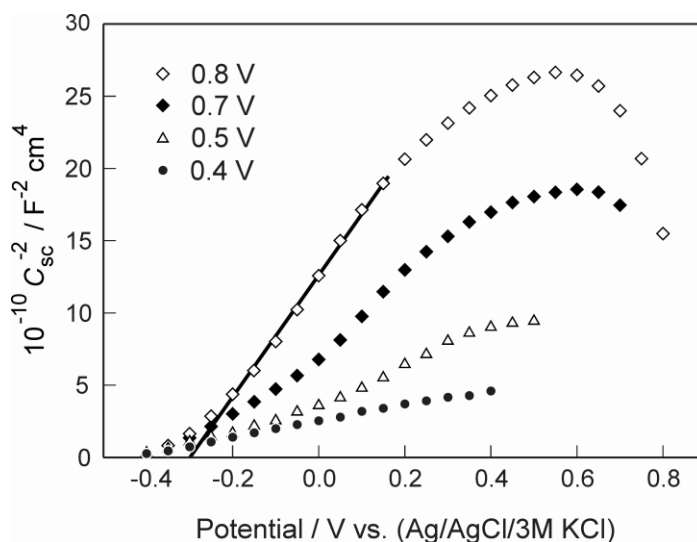


Figure 2. The Mott-Schottky plot for iron passivated at denoted potential values in a borate buffer solution, pH 8.4.

Inside the potential region from 0.40 to 0.80 V the donor density (N_D) value decreases exponentially (from $\sim 9 \times 10^{19} \text{ cm}^{-3}$ to $\sim 1 \times 10^{19} \text{ cm}^{-3}$), following the prediction reported by Sikora et al. [17]:

$$N_D = 3.42 \times 10^{22} \exp(-15.4E_f) + 1.32 \times 10^{22} \tag{4}$$

where the constant w_2 equals to $1.32 \times 10^{22} \text{ cm}^{-3}$. The numerical value of E_{fb} is almost independent of the formation potential and equals to -0.32 V. The N_D values of the same order of magnitude or one order of magnitude higher were reported for iron in the same solution [7,27]. The E_{fb} values approximately the same [27] or about 50 mV more positive [7] were reported in the literature.

3.3. The diffusivity of point defects within the growing passive film on iron

Anodic polarization of iron in a borate buffer solution results in an increase in the film thickness, which takes place via point defect diffusivity inside the oxide layer. The point defect model yields a number of diagnostic criteria that can be used to determine the identity of the principal electronic and crystallographic defects (anion and cation vacancies and metal interstitial), provided that

the passive film is a defect semiconductor [16]. One of these is that the steady state current (j_{ss}) for the anion vacancies (n-type of conductivity) is independent on the applied potential, as was observed for iron in the present study. As an example, the potentiostatic transient, obtained at $E_f = 0.40$ V, is presented in Fig. 3. The passive current density of iron in a borate buffer decreased with time at all potentials investigated, and it was assumed that it reached the steady state value after 24 h. Generally, a time period ranged from 20 to 24 h has been often reported as sufficient to reach the steady state current density [28-30]. Inside the potential region from 0.10 to 0.50 V, the passive current density reached the values $1.6 \pm 0.2 \times 10^{-8}$ A cm⁻², i.e., it was independent of the potential as shown in the insert in Fig. 3.

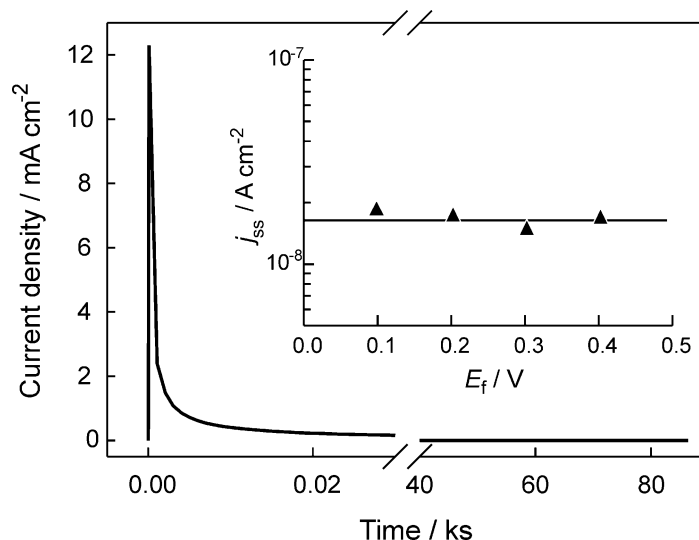


Figure 3. The potentiostatic transient of iron recorded at 0.4 V in a borate buffer solution, pH 8.4. The insert: The dependence of the steady-state passive current densities on the potential of oxide formation.

An independency of j_{ss} on the formation potential indicates that the passive film on iron behaves as an anion conductor due to a preponderance of anion vacancies over cation vacancies. Based on the Nernst-Planck transport equation, Sikora et al. [17] have demonstrated that the diffusivity of oxygen vacancies can be determined from the expression:

$$D_{\text{O}} = -J_{\text{O}}RT / 2F\omega_2H \quad (5)$$

where J_{O} is the steady state flux of oxygen vacancies, ω_2 is the experimental parameter ($\omega_2 = 1.32 \times 10^{22}$ cm⁻³, the section 3.2), H is the mean electric field strength (2.44×10^6 V cm⁻¹ [27]), while R and T have their usual meanings. The steady state flux of double charged oxygen vacancies can be determined from the steady state passive current density; $J_{\text{O}} = -j_{ss}/2e$, where e is the charge of an electron (1.602×10^{-19} C). With $j_{ss} = 1.70 \times 10^{-8}$ A cm⁻², determined from potentiostatic transients, the value of J_{O} equals to 1.32×10^{10} s⁻¹ cm⁻². Substituting the above values into Eq. (5) gives the value for D_{O} equal to 2.1×10^{-17} cm² s⁻¹. The values of the same order of magnitude were reported for passive films on iron in a borate buffer solution, pH, 8.4 [27], and iron in 1M HNO₃ [31]. Generally, the values

of D_0 calculated using the low-field limit are up to two orders of magnitudes higher than those calculated using the high-field limit approximation [32,33].

3.4. Electroreduction of the passive films on iron in a borate buffer solution

MS analysis was also performed at potentials corresponding to the potential region of the current peak A_{II}. As an example, Fig. 4 presents the MS plot obtained with the iron electrode stabilized at the open circuit potential (-0.265 V) for 24 h, and then subjected to the cathodic polarization up to -1.0 V ($v = 50 \text{ mV s}^{-1}$). At potentials corresponding to the anodic current peak A_{II}, the passive film on iron behaves as an n-type semiconductor. The presence of Fe^{3+} interstitials and electrons leads most probably to the appearance of Fe_3O_4 [8].

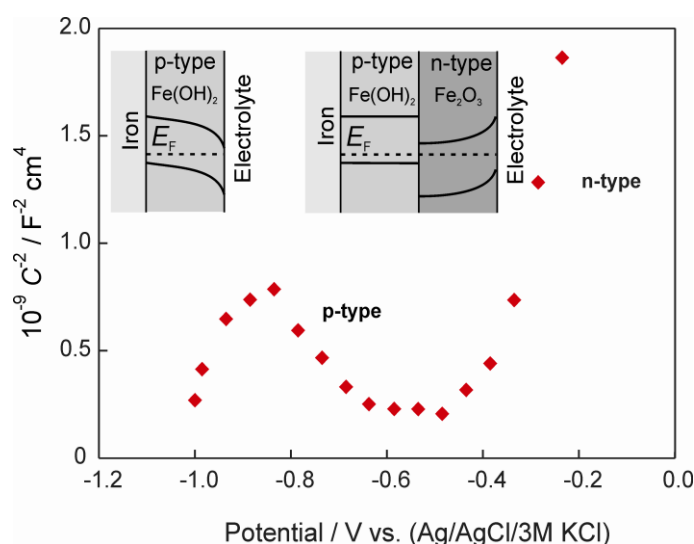


Figure 4. The Mott-Schottky plot for iron passivated at the open circuit potential (-0.265 V) in a borate buffer solution, pH 8.4. The insert: The energy-band diagram model for the solid-state electrochemical processes at the iron oxide|electrolyte interface.

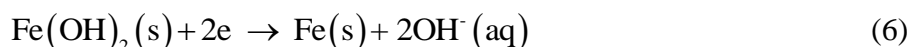
From the C_{sc}^{-2} vs. E slope and Eq. (2) the donor density, $N_D = 1.5 \times 10^{21} \text{ cm}^{-3}$ and the flat band potential, $E_{fb} = -0.4 \text{ V}$ were estimated. Much higher N_D values and disorder of the passive film on iron formed at potentials inside the region of the peak A_{II} in the comparison with N_D values obtained in the passive range of the peak A_{III} have been attributed by many authors to increased concentration of Fe^{2+} inside the passive film [34]. In the passive film formed at nobler potentials, the oxidation of Fe^{2+} to Fe^{3+} takes place and affects the N_D , i.e., the concentration of anion vacancies [35]. Namely, the oxidation of Fe^{2+} to Fe^{3+} is analogous to the substitution of Fe^{3+} ions for Fe^{2+} ions in the film, what creates ionic species (Fe_{Fe}^+) that have an effective charge of +1. Therefore, the overall concentration of Fe^{2+} ions in the passive film is very small.

Inside the potential range between -0.60 and -0.85 V, the MS analysis suggests that the dominant point defects in the surface film become cation vacancies, i.e. iron vacancies, which can give

the reason to the p-type behaviour. The acceptor density (N_A) (due to the p-type behaviour) was $4.7 \times 10^{21} \text{ cm}^{-3}$ and $E_{fb} = -0.60 \text{ V}$ as calculated by using the negative slope of the MS plot (Fig. 4) and Eq. (3).

Based on the MS analysis, a “switch” in the point defect type of the surface film on iron suggests the onset of the surface film reduction (cathodic decomposition) and can be linked to the sudden rise of the current density during the cathodic sweep in Fig. 1. This process occurs at ca. -0.4 V , i.e., close to the E_{fb} value of the passive film formed inside the potential range of the current peak A_{II} . According to the j - E characteristics of the cathodic part of the cyclic voltammogram (Fig. 1) the cathodic reduction process of the passive film is gradual and proceeds in two steps, primarily via a solid-state mechanism. In the first step the potential at which the onset of electroreduction takes place (see Fig. 1) is close to the $E_{fb} = -0.40 \text{ V}$ of the passive layer formed inside the peak A_{II} . Below this potential value there is no surface barrier to electron transport from the metal to the outer layer of the passive film at cathodic potentials. Thus, opposite to an ionic conduction mechanism of the oxide film formation at the metal|film interface, its reduction takes place at the film|solution interface via an electronic conduction mechanism. Electrons injected over a low energy barrier at the metal|film interface being transported to the film|solution interface ($e^-_m \rightarrow e^-_{\text{surface film}}$) where they are trapped in the anion vacancies. Electrons trapped at the film|solution interface cause reduction of the outer Fe_2O_3 layer by the solid state reaction: $\text{Fe(III)(s)} + e^- \rightarrow \text{Fe(II)(s)}$, followed by dissolving of Fe(II) species [1,2,9], which can be considered as a result of the equilibrium displacement: Fe(II) doping species $\leftrightarrow \text{Fe}^{2+}(\text{aq})$.

The second stage of the cathodic decomposition of the surface film commences with an abrupt increase in the cathodic current at potentials below E_{fb} of the Fe(II) film ($E_{fb} = -0.6 \text{ V}$). The appearance of a sharp cathodic current peak C_1 indicates the segregation of a new phase of Fe-metal and can be written as



The nucleation of Fe-metal in the matrix of the Fe(II) film and segregation of the new metal phase occur together with hydrogen evolution [10,36]. Studying the electrochemical behaviour of iron in the system Au|Fe|borate buffer, Diez-Perez et al. [37] have shown that the current peak corresponding to second stage of cathodic reduction, i.e., to Eq (6) is clearly visible because the hydrogen evolution is shifted to the cathodic side for ca. 100 mV in the system investigated.

3.5. Electronic resistances - protecting properties of the passive film and the inhibitor film on iron

The barrier properties of oxide passive films potentiostatically formed on the iron electrode at potential values corresponding to the current peaks A_{II} and A_{III} were investigated using EIS measurements. As an example, Fig. 5 represents the spectra recorded at several potentials inside the potential region from -0.30 to 0.60 V and presented as the Bode plots. All measurements were made on films formed for 24 hours under potentiostatic conditions (see Experimental part).

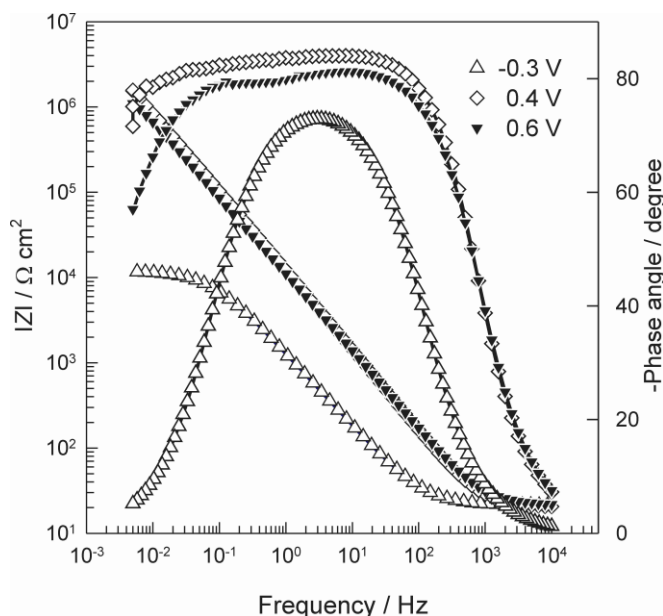


Figure 5. The Bode plot representation of impedance spectra recorded on iron passivated at denoted potential values in a borate buffer, pH 8.4.

The shape of the spectra suggests that the electrode process taking place inside this potential region can be described by a Randles circuit. The numerical values of the EIS parameters are listed in Table 1. The capacitance values of iron passivated at potentials ranging from 0.20 to 0.60 V range from 7 to 10 $\mu\text{F cm}^{-2}$ (Table 1), and are typical for the passive iron and steel electrodes in near neutral and slightly alkaline solutions [7,22,27]. An increase in the passive film capacitance is observed below 0.20 V. The values of charge transfer resistance (R_{ct}) point to the excellent barrier properties of iron oxide in a borate buffer, pH 8.4, especially at potential values from 0.2 to 0.5 V. The small difference in the impedance in the passive range is in agreement with prediction of point defect model (PDM).

Table 1. Numerical values of impedance parameters obtained for iron passivated at denoted potential values in a borate buffer solution, pH 8.4.

E_f / V	-0.3	-0.2	-0.1	0.0	0.2	0.3	0.4	0.5	0.6
$R / \text{k}\Omega \text{ cm}^2$	12	22	36	612	4.3×10^3	3.3×10^3	8.8×10^3	6.6×10^3	2.5×10^3
$C / \mu\text{F cm}^{-2}$	73	60	47	21	8.6	9.5	8.7	7.1	7.7

Since the electric field strength within the film is viewed to be constant over the passive range, the impedance should be independent of the film thickness or formation potential [16]. A decrease in the R_{ct} values occurred by decreasing the E_f value below 0.0 V points to a significant decrease in barrier properties of the passive film. Since the open circuit potential (E_{OCP}) of iron in an aerated borate buffer solution, pH 8.4, establishes inside the potential region between -0.3 and -0.2 V, it is evident that the corrosion resistance of iron in this solution is very low, and protection of iron as well as the carbon steels in near neutral solutions is needed.

As the isoelectric point of hydrated surface of iron oxide inside this potential region is at $\text{pH} < 8$ [38], the adsorption of ionic liquid cations was supposed to occur spontaneously and that it might protect iron in slightly alkaline solutions. To check this possibility, the inhibiting action of the imidazolium cations ($[\text{C}_4\text{Mim}]^+$) on iron corrosion was investigated. The impedance measurements were performed with iron immersed into a borate buffer solution, $\text{pH} 8.4$, containing 7 mM of $[\text{C}_4\text{Mim}]^+\text{Br}^-$ ionic liquid during a period of 24 h . The spectra presented in Fig. 6 as Bode plots, show a significant increase in the low-frequency impedance modulus, which indicates an increasing corrosion resistance of the surface film formed by adsorption of $[\text{C}_4\text{Mim}]^+$ cations onto the iron surface.

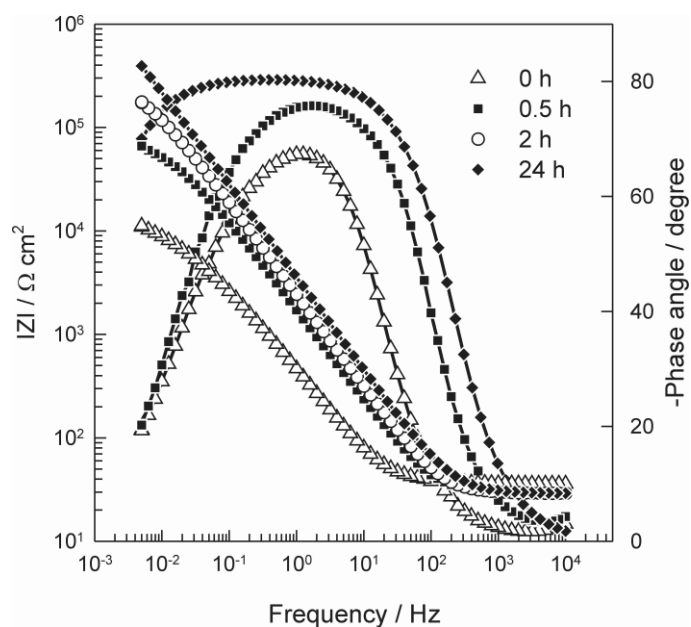


Figure 6. The Bode plot representation of impedance spectra recorded on iron at denoted immersion periods in a borate buffer, $\text{pH} 8.4$, containing 7.0 mM 1-butyl-3-methylimidazolium bromide.

All spectra are characterized by a single time constant, and were fitted to the Randles circuit. The numerical values of impedance parameters, listed in Table 2, show that adsorption of $[\text{C}_4\text{Mim}]^+$ ions has caused an increase in the R_{ct} value for two orders of magnitude. The protection efficiency percentage (PE%) of ionic liquid was calculated using the expression:

$$\text{PE} / \% = \left[\left(R_{\text{ct,IL}} - R_{\text{ct}} \right) / R_{\text{ct,IL}} \right] \times 100 \quad (7)$$

where R_{ct} and $R_{\text{ct,IL}}$ represent the charge transfer resistance of iron in a borate buffer solution alone and in the presence of ionic liquid, respectively. The value obtained was 99.4% . Data in Table 2 also show that during the immersion period of 24 h , the E_{OCP} value moved to the positive side for about 100 mV . The results obtained confirm that during a prolong immersion time the excess of negative surface charge decreases and the surface layer becomes more compact in structure (aging effects).

Table 2. Numerical values of impedance parameters obtained for iron in a borate buffer solution, pH 8.4, containing 7 mM [C₄MIm]⁺ Br⁻ ionic liquid at denoted immersion time.

<i>t</i> / h	<i>E</i> _{OCP} / V	<i>R</i> / kΩ cm ²	<i>C</i> / μF cm ⁻²
0	-0.265	11	205
0.5	-0.222	66	52
1	-0.208	131	45
2	-0.200	243	39
3	-0.194	345	36
4	-0.189	464	34
5	-0.157	622	33
21	-0.162	1950	19
24	-0.147	2090	28

3.6. Chemical composition of the passive films on iron - X-ray photoelectron spectroscopy

XPS spectra were recorded around iron and oxygen core-levels on the passivated iron samples with the aim to determine the composition of the surface film in the potential regions of the current peaks A_{II} and A_{III} (see Fig. 1).

Fig. 7 shows the photoemission spectra around O 1s and Fe 2p_{3/2} core-levels taken from the iron surface passivated at +0.4 V. This potential value was chosen because it falls near the center of the stable passive region of the current peak A_{III}. Fig. 7 also shows XPS results collected at -0.4 V. This potential value falls at the beginning of the region of the current peak A_{II}, see Fig. 1. To identify changes in chemical composition of the surface passive film, during cathodic polarization, the potential was swept ($\nu = 50 \text{ mV s}^{-1}$) from +0.4 V (after 2 hours polarization) up to -0.4 V and the electrode was withdrawn from the solution. In both cases, the samples were rinsed with deionized water, dried with air, and finally transferred to the XPS vacuum chamber.

XPS spectra of both investigated iron samples have showed two main constituents, Fe and O. In addition, the survey XPS spectra have also shown the presence of several contaminants, such as carbon, silicon and nitrogen picked up from the surface preparing, atmosphere and the UHV environment.

As can be seen from Fig. 7, for both samples O 1s emission peaks were deconvoluted into four contributions (solid lines in Fig. 7). We assign the dominant peak at binding energy (BE) of 530 eV to the oxygen (O²⁻) from an iron oxide. Three other, less intensive contributions at BEs of 531.25, 532.1 and 533.5 eV have been assign previously to OH⁻, C-O/O-C=O and H₂O species [39]. In Fig. 7 we note a substantial increase in intensity of OH⁻-related peak in iron passivated at -0.4 V, leading to the decrease of O²⁻/OH⁻ ratio from 3.5 to 2.6 in samples passivated at 0.4 V and -0.4 V, respectively.

In the case of Fe 2p_{3/2} emission, we assign the component at BE of 506.6 eV to the bulk metal, Fe⁰ indicating that the surface film is thin enough to allow photoelectrons, originating from the bulk metal, to be detected. The components at BEs of 509.85 and 511.75 eV are assigned to two different oxidation states of iron, Fe³⁺ and Fe²⁺ [39], in the form of surface oxides and hydroxides, respectively

[39,40]. The binding energy values for Fe^0 , Fe^{2+} and Fe^{3+} peaks are in agreement with the literature values [39,40].

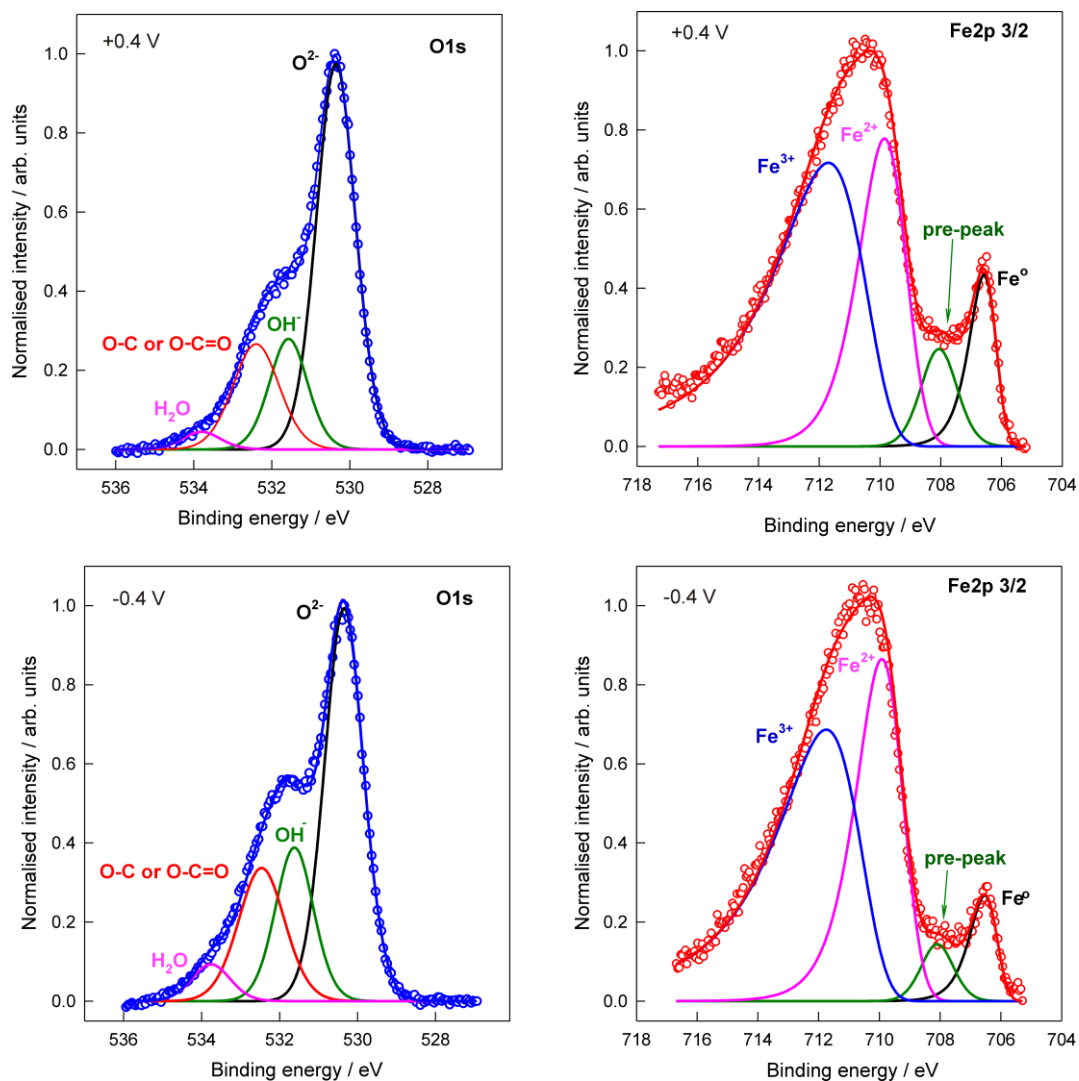


Figure 7. The deconvoluted XPS spectra of O 1s and Fe 2p_{3/2} electrons obtained for the iron samples passivated at 0.4 V and -0.4 V.

It is known, that the analysis of the XP spectra of the iron core level Fe 2p line is complicated because of spin-orbit coupling, multiple oxidation states and satellites associated with the different oxidation states [39]. Therefore, to achieve the best fit of experimental curves in Fig.7, an additional, low intensity pre-peak is required at BE of 708.1 eV [41], while the multiplet splitting effects of Fe^{3+} and Fe^{2+} states [39] were simulated by asymmetric tail at high energy sides of Fe 2p peaks [39].

Different values of $\text{Fe}^{3+}/\text{Fe}^{2+}$ ratio were found for samples in Fig.7: 1.8 for the sample passivated at 0.4 V and 1.4 for the sample passivated at -0.4 V. This difference can be attributed to the increased contribution of $\text{Fe}(\text{OH})_2$ in iron films passivated at -0.4 V, in full agreement with our O 1s spectra from Fig.7.

4. CONCLUSIONS

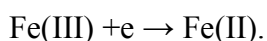
To predict the long-term corrosion properties of iron, a deep understanding of the electronic properties of the surface films is needed. The electronic structure of the surface protecting film on iron was discussed in terms of structural sensitive parameters such as low-frequency resistance, high-frequency capacitance, and phase angle determined *in situ* from EIS measurements and correlated with the corrosion resistance.

The band structure model was employed to identify the stoichiometric defects and to explain the kinetics of oxide film growth. It was assumed that the depletion region in the film close to the film|electrolyte interface dominates electronic properties of the passive film, which behaves as n-type semiconductor. The anion diffusion coefficient was extracted from the relationship between the donor density and the transport equation for low-field approximation growth law of the oxide film formation.

A low value of diffusion coefficient and high values of the charge transfer resistance point to the high corrosion resistance and protecting properties of the passive oxide film in the wide range of potentials. The protecting efficiency of the spontaneously formed oxide film at the open circuit potential was markedly enhanced by adsorption of imidazolium cations. After an immersion period of 24 h, the protection efficiency of adsorbed inhibitor is above 99%.

It was shown that the electronic properties of the bilayer passive film on iron have a strong influence on its cathodic reduction (decomposition) up to metallic iron. The kinetics of the overall reduction reaction, regarded as a two step process, was limited by the height of the potential barrier at the metal|film or film|solution interface and the energy level of the dopand (traps) in the forbidden gap.

The first step: the reduction of the outer part of the passive film takes place at the film|solution interface. The kinetics of this step is determined by a low barrier at the metal|film interface and the energy level of anion vacancies. Dissolution of Fe(II) species follows solid-state reaction:



The second step: the reduction of the inner Fe(II) hydroxide layer into metallic Fe takes place together with the hydrogen evolution reaction with kinetics determined by energy level of cation vacancies and the high of the Schottky barrier at the film|solution interface.

According to the XPS results the structure and the chemical composition of the oxide film depend on the formation potential. Species observed in passive films of samples treated at both 0.4 and -0.4 V include Fe⁰, Fe²⁺, and Fe³⁺. The Fe³⁺/Fe²⁺ ratio equals to 1.8 and 1.4 for samples passivated at 0.4 V and -0.4 V, respectively. Thus, an overall description of the surface film composition would be: the increased contribution of Fe(OH)₂ in the surface film formed at -0.4 V, i.e. in the “low passive range” (region of the peak A_{II}), and predominantly contribution of Fe₂O₃ in the “high passive range” (region of the peak A_{III}) what is in a full agreement with O 1s spectra.

ACKNOWLEDGEMENTS

The financial support provided by the Ministry of Science, Education and Sports of the Republic of Croatia within the research grant 125-0982904-2923 is greatly appreciated. The authors are grateful to Dr. sc. Ranko Babić for his valuable discussion.

References

1. M. Nagayama and M. Cohen, *J. Electrochem. Soc.*, 109 (1962) 781
2. M. Nagayama and M. Cohen, *J. Electrochem. Soc.*, 110 (1963) 670
3. M. Büchler, P. Schmuki and H. Böhni, *J. Electrochem. Soc.*, 145 (1998) 609
4. I. Díez-Pérez, P. Gorostiza, F. Sanz and C. Müller, *J. Electrochem. Soc.*, 148 (2001) B307
5. V. Jovancicevic, R. C. Kainthla, Z. Tang, B. Yang, and J. O'M. Bockris, *Langmuir*, 3
6. (1987) 388
7. M. Bojinov, G. Fabricius, T. Laitinen, K. Mäkelä, T. Sario and G. Sundholm, *Electrochim. Acta*, 45 (2000) 2029
8. S. P. Harrington, F. Wang and T. M. Devine, *Electrochim. Acta*, 55 (2010) 4092
9. A. J. Davenport, L. J. Oblonsky, M. P. Ryan and M. F. Toney, *J. Electrochem. Soc.*, 147
10. (2000) 2162
11. I. V. Sieber, H. Hildebrand, S. Virtanen and P. Schmuki, *Corros. Sci.*, 48 (2006) 3472
12. M. E. Vela, J. R. Vilche and A.J. Arvia, *J. Appl. Electrochem.*, 16 (1986) 490
13. U. Stimming and J. W. Schultze, *Electrochim. Acta*, 24 (1979) 859
14. N. Sato, K. Kudo and T. Noda, *Electrochim. Acta*, 16 (1971) 1909
15. Z. Lu and D. D. Macdonald, *Electrochim. Acta*, 53 (2008) 7696
16. K. Azumi, T. Ohtsuka, N. Sato, *J. Electrochem. Soc.*, 134 (1987) 1352
17. D. D. Macdonald, *Pure Appl. Chem.*, 71 (1999) 951
18. D. D. Macdonald, *J. Electrochem Soc.*, 139 (1992) 3434
19. E. Sikora, J. Sikora and D. D. Macdonald, *Electrochim. Acta*, 41 (1996) 783
20. E. P. Friis, J. E. T. Andersen, L. L. Madsen, N. Bonander, P. Moller and J. Ulstrup,
21. *Electrochim. Acta*, 43 (1998) 1114
22. A. Boukamp, *Solid State Ionics*, 20 (1986) 31
23. J. -B. Jorcin, M. E. Orazem, N. Pebere and B. Tribollet, *Electrochim. Acta*, 51 (2006) 1473
24. G. J. Brug, A. L. G. van der Eeden, M. Sluyters-Rehbach and J.H. Sluyters, *J. Electroanal. Chem.*,
25. 176 (1984) 275
26. Ž. Petrović, M. Metikoš-Huković and R. Babić, *Electrochim. Acta*, 75 (2012) 406
27. S. P. Harrington and T. M. Devine, *J. Electrochem. Soc.*, 155 (2008) C38
28. T. Misawa, *Corros. Sci.*, 13 (1973) 659
29. S. R. Morrison, *Electrochemistry at Semiconductor and Oxidized Metal Electrodes*,
30. Plenum Press, New York (1980)
31. J. Liu and D. D. Macdonald, *J. Electrochem. Soc.*, 148 (2001) B425
32. S. J. Ahn and H.S. Kwon, *J. Electroanal. Chem.*, 579 (2005) 311
33. Z. Grubač, Ž. Petrović, J. Katić, M. Metikoš-Huković and R. Babić, *J. Electroanal. Chem.*, 645
34. (2010) 87
35. M. Metikoš-Huković, R. Babić, Z. Grubač, Ž. Petrović and N. Lajçi, *Corros. Sci.*, 53 (2011) 2176
36. K. -J. Park, A. -Jin Ahn and H. -S. Kwon, *Electrochim. Acta*, 56 (2011) 1662
37. X. P. Guo, Y. Tomoe, H. Imaizumi and K. Katoh, *J. Electroanal. Chem.*, 445 (1998) 95
38. M. Bojinov, G. Fabricius, T. Laitinen, K. Makela, T. Saario and G. Sundholm, *Electrochim. Acta*,
39. 46 (2001) 1339
40. G. Vasquez and I. Gonzales, *Electrochim. Acta*, 52 (2007) 6771
41. S. Virtanen, P. Schmuki, H. Bohni, P. Vuoristo and T. Mantyla, *J. Electrochem. Soc.*, 142 (1995)
42. 3067
43. S. J. Ahn and H.S. Kwon, *Electrochim. Acta*, 49 (2004) 3347
44. I. Díez-Pérez, F. Sanz and P. Gorostiza, *Electrochem. Commun.*, 8 (2006) 1597
45. I. Díez-Pérez, P. Gorostiza, M.-C. Bernard, P. Allongue and F. Sanz, *Probing the passivity of iron by electrochemical scanning tunneling microscopy and spectroscopy*, Thesis, 2006, chapter 3.3, p.143

43. M. Kosmulski, *J. Colloid Interface Sci.*, 337 (2009) 439
44. G. Bhargava, I. Gouzman, C. M. Chun, T. A. Ramanarayanan and S. L. Bernasek, *Appl. Surf. Sci.*, 253 (2007) 4322
45. L. A. Toledo-Matos and M. Pech-Canul, *J. Solid State Electrochem.*, 15 (2011) 1927
46. A. P. Grosvenor, B. A. Kobe, M. C. Biesinger and N. S. McIntyre, *Surf. Interface Anal.*, 36 (2004) 1564